High-cycle fatigue of Ti–6Al–4V

R. O. RITCHIE, D. L. DAVIDSON[1], B. L. BOYCE, J. P. CAMPBELL and O. RODER

Department of Materials Science and Mineral Engineering, University of California, Berkeley, CA 94720-1760, USA, [1]Southwest Research Institute, P.O. Drawer 28510, 6220 Culebra Road, San Antonio, TX 78228-0510, USA

ABSTRACT The definition of the critical levels of microstructural damage that can lead to the propagation of fatigue cracks under high-cycle fatigue loading conditions is a major concern with respect to the structural integrity of turbine-engine components in military aircraft. The extremely high cyclic frequencies characteristic of in-flight loading spectra, coupled with the presence of small cracks resulting from fretting or foreign object damage (FOD), necessitate that a defect-tolerant design approach be based on a crack-propagation threshold. The present study is focused on characterizing such near-threshold fatigue-crack propagation behaviour in a Ti–6Al–4V blade alloy (with $\sim$60% primary α in a matrix of lamellar $\alpha+\beta$), at high frequencies (20–1500 Hz) and load ratios (0.1–0.95) in both ambient temperature air and vacuum environments. Results indicate that 'worst-case' thresholds, measured on large cracks, may be used as a practical lower bound to describe the onset of naturally initiated small-crack growth and the initiation and early growth of small cracks emanating from sites of simulated FOD.

Keywords high-cycle fatigue; crack propagation; foreign object damage; fatigue thresholds; small cracks; titanium alloys.

INTRODUCTION

High-cycle fatigue (HCF) has been identified as one of the prime causes of turbine-engine failure in military aircraft.[1] It can result in essentially unpredictable failures due to the propagation of fatigue cracks in blade and disk components under ultrahigh-frequency loading, where the cracking initiates from small defects often associated with microstructural damage caused by fretting or foreign object impacts.[2] To prevent HCF failures, design methodologies are required that identify the critical levels of microstructural damage which can lead to such failures. The current study is focused on identifying these critical levels of damage and in characterizing fatigue behaviour under representative operating conditions in a Ti–6Al–4V alloy, typically used in the front, low-temperature stages of the engine.

During HCF, engine components experience high-frequency ($\sim$1–2 kHz) vibrational loads due to resonant airflow dynamics, often superimposed on a high mean stress,[2,3] although the exact source and magnitude of the stresses remains uncertain. Because of the high frequencies, even cracks growing at slow per-cycle velocities (i.e. $\sim 10^{-10}$–10^{-9} m/cycle) propagate to failure in a short period of time; consequently, HCF-critical turbine components must be operated below the fatigue-crack propagation threshold (ΔK_{TH}) such that crack propagation cannot occur (within $\sim 10^9$ cycles). An extensive database (e.g. Refs [4,5]) exists for such thresholds; however, it has been largely derived from standard test geometries containing large (> few mm) through-thickness cracks, often under loading conditions that may not be representative of turbine-engine HCF. Furthermore, except under specific loading conditions, e.g. at high mean loads, as discussed below, such tests are not necessarily relevant to the HCF problem, where the critical flaw sizes are much smaller, i.e. <500 μm.[6] Because small cracks can grow at velocities faster than corresponding large cracks (at the same applied driving force) and can propagate below the large-crack ΔK_{TH} threshold, design against HCF failure must be based on the notion of a practical small-crack threshold, measured under the representative conditions.[7]

The principal reasons why small cracks behave differently from large cracks are associated with crack sizes becoming comparable to: (i) microstructural size scales, where biased sampling of the microstructure leads to accelerated crack advance along 'weak' paths (a continuum limitation); (ii) the extent of local plasticity ahead of the crack tip, where the assumption of small-scale

yielding implicit in the use of the stress intensity, K, is not strictly valid (a linear-elastic fracture mechanics limitation); and (iii) the extent of crack-tip shielding (e.g. by crack closure) behind the crack tip, where the reduced role of shielding leads to a higher local driving force than the corresponding large crack at the same applied ΔK (a similitude limitation).[8]

Of these three classes of small cracks, we believe that the latter (the physically small crack) is most important in the present case, as cyclic plastic-zone sizes will generally not exceed a few micrometres, and the crack sizes relevant to the aircraft HCF problem are invariably much larger than the characteristic microstructural dimensions. However, as it would be difficult to design engine components on the basis of small-crack results, simulating such results using a reproducible large-crack technique would appear to offer a feasible and practical solution. The philosophy here is that as the relevant crack sizes in HCF are not small compared to microstructural size-scales or the dimensions of local inelasticity, then the principal difference between large and small cracks lies in the degree of crack-tip shielding present in the crack wake. Thus, by performing large-crack tests where the extent of crack closure behind the crack tip is minimized, it is reasoned that a worse-case large-crack threshold can be measured which would reflect the behaviour of physically small cracks. It should be emphasized that such procedures will not work where crack sizes become small compared to microstructural dimensions.

Accordingly, in the present work, we compare fatigue threshold values and the near-threshold crack growth rate behaviour of large (>5 mm) through-thickness cracks, naturally initiated small ($\sim$45–1000 μm) cracks, and small (<500 μm) surface cracks initiated from artificially induced notches and from sites of simulated foreign object damage (FOD), in a single microstructure of Ti–6Al–4V, tested at high frequencies ($\sim$50–1500 Hz) and load ratios ($R \sim 0.1$–0.95) in both room air and vacuum environments. In addition to seeking insight into the mechanisms of crack growth under these conditions, we examine whether 'worst-case' threshold values, measured for the large cracks using standard test geometries subject to special loading conditions, can have any utility as a practical lower bound for the onset of small-crack growth under HCF conditions.

EXPERIMENTAL PROCEDURES

Material and microstructure

A Ti–6Al–4V alloy, with a composition (in wt%) of 6.30Al, 4.17V, 0.19Fe, 0.19O, 0.013N, bal. Ti, was supplied from a set of forgings produced specifically for the US Air Force sponsored program on HCF. The bar-stock, originating from Teledyne Titanium, was forged into 400 × 150 × 20 mm plates and subsequently solution-treated at 925 °C (1 h) and vacuum-annealed at 700 °C (2 h) for stabilization. The microstructure consisted of a bimodal distribution of $\sim$60 vol.% primary-α and $\sim$40 vol.% lamellar colonies of α + β (Fig. 1), with a tensile strength of 970 MPa, a yield strength of 926–935 MPa and a Young's modulus of 116 GPa (based on tensile tests conducted along the longitudinal axis at a strain rate of $5 \times 10^{-4}\ s^{-1}$).[9]

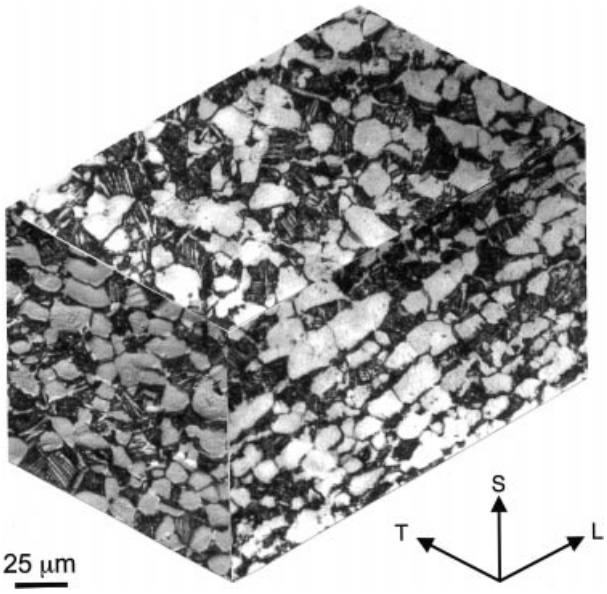

Fig. 1 Optical micrograph of the microstructure of the solution-treated and overaged Ti–6Al–4V studied. The microstructure consists of ≈60% primary α and 40% lamellar α + β colonies. The grains were slightly elongated along the L forging axis. All fatigue specimens were extracted in the L–T orientation (such that the crack surface was in the S–T plane and the crack propagated in the T direction). (Etched in Kroll's solution.)

To minimize residual stresses in this material, all small-crack test samples were machined using low-stress procedures, and chemically milled or electropolished to remove $\sim$30–100 μm of material.

Fatigue-crack propagation testing

Large-crack testing

Large-crack propagation studies were conducted in ambient temperature air on compact-tension C(T) specimens machined in the L–T orientation (8 mm thick, 25 mm wide) at R ratios (ratio of minimum to maximum loads) varying from 0.10 to 0.95 in a lab air environment (22 °C, $\sim$45% relative humidity). Crack lengths were monitored *in situ* using the back-face strain compliance

technique, and were verified periodically by optical inspection. Macroscopic levels of crack closure were also monitored using back-face strain compliance; specifically, the (global) closure stress intensity, K_{cl}, was approximated from the closure load, measured at the point of first deviation from linearity in the elastic compliance curve upon unloading.[10]

To approach the threshold, both constant and variable *R*-testing was employed. Under both conditions, loads were shed such that $\Delta K = \Delta K_{initial} \exp[C(a - a_{initial})]$, with the normalized *K*-gradient, *C*, set to $-0.08\ mm^{-1}$, as suggested in ASTM Standard E-647 (ΔK is the stress-intensity range and *a* is the crack length). With variable *R*-testing, the threshold was approached under constant K_{max}/increasing K_{min} conditions to minimize the effect of crack closure.[11,12] At 50–200 Hz (sine wave), tests were conducted on conventional MTS servo-hydraulic testing machines operating under automated closed-loop *K* control, with the fatigue thresholds, ΔK_{TH} and $K_{max,TH}$, defined as the minimum values of these parameters yielding a propagation rate of 10^{-10} m/cycle. Corresponding fatigue tests at 1000 Hz were performed under *K* control on a newly developed MTS servo-hydraulic test frame using a voice-coil servovalve; details of this instrument are described elsewhere.[13] At the higher frequencies, thresholds could be readily defined at a lower propagation rate of 10^{-11} m/cycle.

Results are presented in the form of the crack growth increment per cycle, d*a*/d*N*, plotted as a function of the applied stress-intensity range, $\Delta K = K_{max} - K_{min}$. Where the effect of closure is considered, growth rates are alternatively plotted in terms of the effective (near-tip) stress-intensity range, $\Delta K_{eff} = K_{max} - K_{cl}$.

Small-crack testing

Specifically to investigate the mechanistic aspects of HCF cracking in this alloy, small (<750 μm) surface crack tests were performed *in vacuo* ($\sim 10^{-6}$ torr) on tensile samples (44 mm long with a 12.5 × 3.2 mm rectangular cross-section) at ~1.5 kHz with load ratios between 0.20 and 0.85 in a specially designed magnetostrictive loading stage for the scanning electron microscope (SEM). Cracks were initiated in three-point bending at artificial notches, generated either using electro-discharge machining (~250 μm in diameter, 250 μm deep) or focused ion beam milling (~30 μm long, 5 μm wide, 30 μm deep).

In addition, the growth rates of small surface cracks initiated from sites of simulated FOD were examined at an applied maximum stress of 500 MPa (at $R = 0.1$ with a frequency of 20 Hz) using cylindrical (buttonhead) tensile specimens containing a rectangular gauge section. The damage was obtained by firing 3.2-mm-diameter, chrome-hardened steel spheres, using compressed gas, onto the flat specimen surface, which had previously been stress relieved and chemically milled to give a nominally stress-free surface. In this study, normal impacts (i.e. incident path orthogonal to the sample surface) were performed at velocities between ~200 and 300 m/s, representing typical in-service impact velocities on blades.

The initiation and growth of such small cracks was measured in the SEM, either *in situ* with the notched tensile specimens or periodically with the simulated FOD specimens. Stress intensities characterizing such crack growth were computed from the Newman–Raju semielliptical surface crack solution,[14] assuming a half-surface length to depth ratio of 0.9–1 (based on fractographic observations).

RESULTS AND DISCUSSION

Large-crack behaviour

Effect of load ratio

The effect of load ratio ($R = 0.1$–0.8) on the fatigue-crack propagation rates of large (>5 mm) cracks, shown in Fig. 2 for Ti–6Al–4V at 50 Hz, indicates (as expected) that higher load ratios induce lower ΔK_{TH} thresholds and faster growth rates at a given applied ΔK level. Threshold stress intensity ranges varied from $4.6\ MPa\sqrt{m}$ at $R = 0.1$ to $2.6\ MPa\sqrt{m}$ at $R = 0.8$. A two-parameter fit of the Paris regime yields a growth

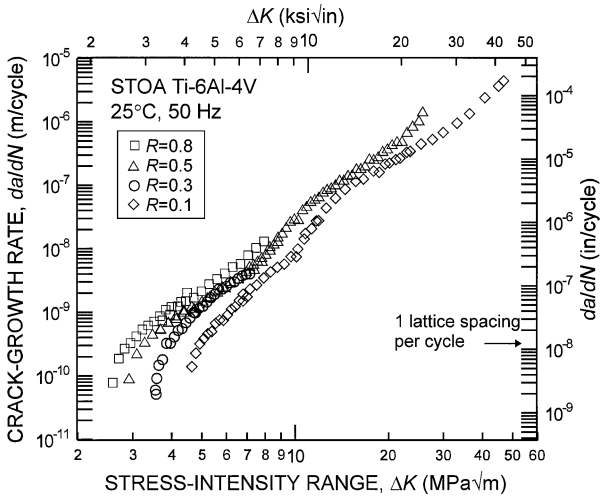

Fig. 2 Fatigue-crack propagation behaviour (large-crack), in the form of growth rates, d*a*/d*N*, as a function of the applied stress intensity range, ΔK, for a solution-treated and overaged Ti–6Al–4V in room air at $R = 0.1$, 0.3, 0.5 and 0.8 (at 50 Hz frequency). ΔK_{TH} fatigue thresholds, measured at growth rates of 10^{-10} m/cycle, were 4.6, 3.6, 2.9 and $2.6\ MPa\sqrt{m}$, respectively.

law of (units: m/cycle, MPa$\sqrt{\text{m}}$):

$$\frac{da}{dN} = 5.2 \times 10^{-12}\, \Delta K^{2.5} K_{max}^{0.67} \quad (1)$$

The observed effect of load ratio is commonly attributed to the role of crack closure, which in Ti alloys is primarily associated with the roughness-induced mechanism (i.e. arising from the wedging of crack-surface asperities, e.g. Refs [15–17]). To examine this, closure stress intensity values, K_{cl}, were measured globally at each load ratio using back-face strain compliance. No detectable (global) closure was observed at $R = 0.5$ and 0.8; however, at $R = 0.1$, K_{cl} values were observed to be roughly constant at ~ 2.0 MPa$\sqrt{\text{m}}$ [Fig. 3(a)]. In Fig. 3(b), the results of Fig. 2 are replotted in terms of the effective stress-intensity range, after accounting for such closure. It is apparent that, similar to previous studies in this alloy,[18] characterizing growth rates in terms of ΔK_{eff} reduces the disparity in crack-growth behaviour between the four R ratios, implying that an important origin of the load ratio effect is indeed crack closure. However, above $R \sim 0.5$ where the role of closure is presumed to be minimal, near-threshold crack-growth rates continue to increase somewhat, and ΔK_{TH} thresholds continue to decrease, with increasing R (see also Fig. 6). This indicates that there may be additional mechanisms, independent of global closure and apparently both K_{max} and ΔK related, which are responsible for the load ratio effect at very high R-values. Alternatively, the effect may be due to the presence of local (near-tip) crack closure which cannot be detected using global methods, e.g. back-face strain compliance. Indeed, such local closure has been detected in microscopy studies, as described below.

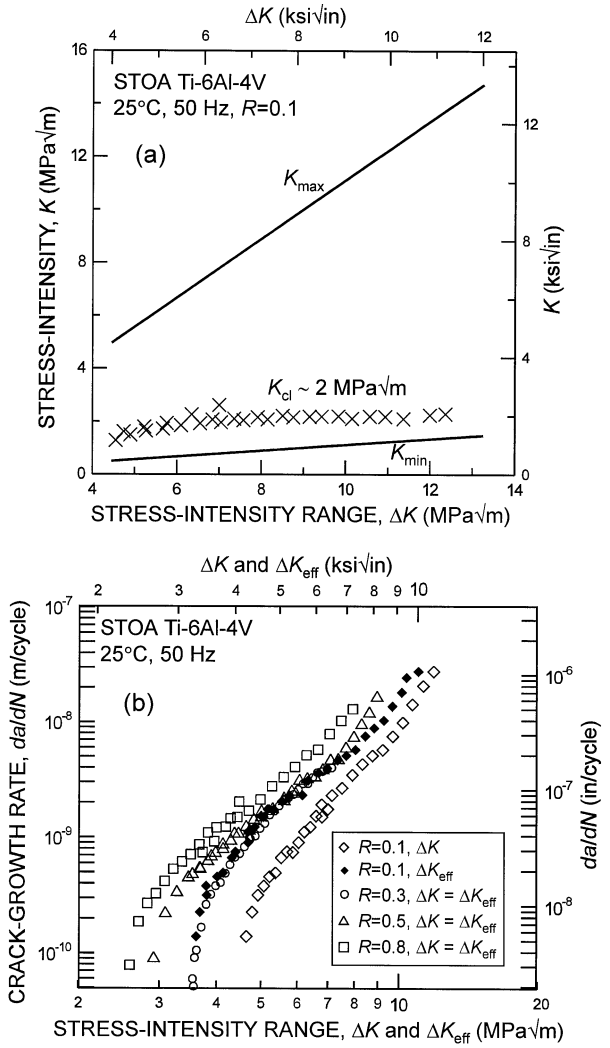

Fig. 3 Crack closure considerations: (a) closure, measured by unloading compliance, stays approximately constant at $K_{cl} \sim 2$ MPa$\sqrt{\text{m}}$; (b) crack growth rates in terms of ΔK_{eff} ($= K_{max}$–K_{cl}) showing the effect of load ratio between $R = 0.1$ and 0.5 is far less pronounced.

The measured variation with load ratio of the threshold ΔK_{TH} and $K_{max,TH}$ values, plotted in Fig. 4, can be compared with the simple closure model of Schmidt and Paris.[19] This model is based on the notion that K_{cl} and the effective ΔK threshold, $\Delta K_{eff,TH}$, are constant and independent of R; it predicts that measured ΔK_{TH}

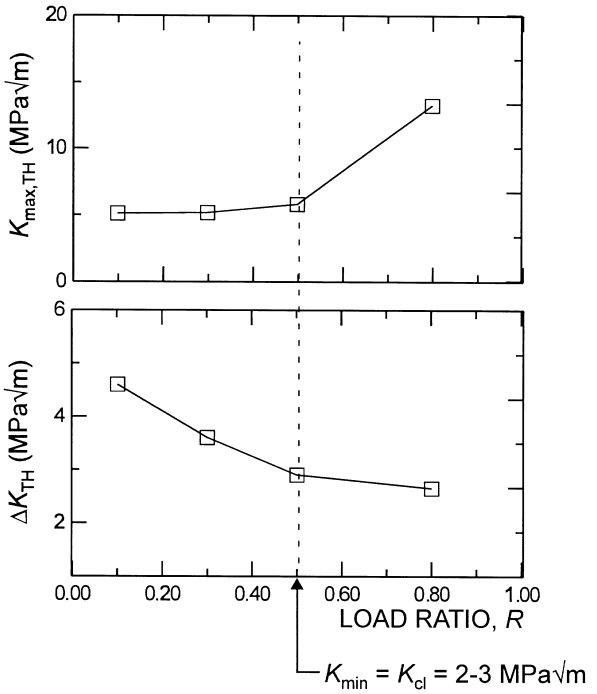

Fig. 4 The variation of $K_{max,TH}$ and ΔK_{TH} with load ratio appears to follow the Schmidt and Paris closure model.[19] Although more data are required to clearly establish a transition, the results presented here show a change in slope at $R \approx 0.5$, consistent with a K_{cl} value of 2–3 MPa$\sqrt{\text{m}}$, similar to that measured directly from test samples using unloading compliance techniques.

and $K_{max,TH}$ thresholds will be load ratio independent, respectively, above and below a transition R at which point $K_{min} = K_{cl}$. Although clearly there are insufficient data to verify this analysis, the present constant-R results are consistent with this model, and the transition R, above which closure is ineffective ($K_{min} > K_{cl}$), is observed at $K_{min} = K_{cl} \approx 2$–$3$ MPa$\sqrt{m}$. Such an estimate of K_{cl} is consistent with the experimentally measured values [Fig. 3(a)] determined from back-face strain compliance.

Effect of frequency

The role of cyclic frequency is shown in Fig. 5, where the growth rates at 50 Hz are compared with data collected at 1000 Hz (at UCB) and 1100–1500 Hz (at SWRI). It is clear that the high-frequency results are not statistically distinguishable from the conventional frequency data. Additional limited experiments at 200 Hz (performed on a conventional servohydraulic machine) and 20 000 Hz (performed by Bathias and co-workers[20] using ultrasonic fatigue testing on a similar microstructure) confirmed this lack of a frequency effect on ambient temperature growth rate behaviour in Ti–6Al–4V. The absence of frequency-dependent growth rates for titanium alloys tested in air over the range 0.1–50 Hz has been reported previously in the literature;[21,22] the current work extends this observation for Ti–6Al–4V to beyond 1000 Hz.

Testing at high frequencies permits thresholds to be defined at lower growth rates. Using the ASTM standard K-gradient of 0.08 mm^{-1}, measurements down to 10^{-11} m/cycle may require several weeks at 50 Hz, whereas these same measurements can be obtained in a single day at 1000 Hz and within a few hours at 20 000 Hz. In the present study, thresholds measured at $\sim 10^{-11}$–10^{-12} m/cycle (at 1000 Hz or above) were found to be ~ 0.1–0.2 MPa$\sqrt{m}$ lower than the 10^{-10} m/cycle thresholds measured at any frequency.

Effect of loading sequence

In an attempt to measure 'lower-bound' thresholds, i.e. at very high R-values where the effect of crack closure is minimized, additional variable R testing was performed at 1000 Hz using constant K_{max}/increasing K_{min} loading sequences (Fig. 6). Here, at a constant K_{max} of 26.5 MPa$\sqrt{m}$, a final load ratio of $R = 0.92$ was achieved, yielding a threshold of 2.2 MPa$\sqrt{m}$; with a constant K_{max} of 36.5 MPa$\sqrt{m}$, a threshold of $\Delta K_{TH} =$ 1.9 MPa$\sqrt{m}$ was achieved with a final load ratio of $R =$ 0.95. These values should be compared to a ΔK_{TH} value of 2.6 MPa$\sqrt{m}$ for constant $R = 0.8$ testing. It should be noted that the effect of closure is expected to be minimal here as the high load ratios result in an extremely large minimum crack-tip opening displacement ($CTOD_{min} \approx 0.6$ and 8.0 μm for $R = 0.8$ and 0.95, respectively), as computed from the numerical analysis of Shih.[23]

The ΔK_{TH} threshold value of 1.9 MPa$\sqrt{m}$ measured under constant K_{max}/increasing K_{min} cycling at $R = 0.95$ is considered to represent the lowest threshold for large cracks measured to date in Ti–6Al–4V. It should be compared with measurements on naturally initiated small

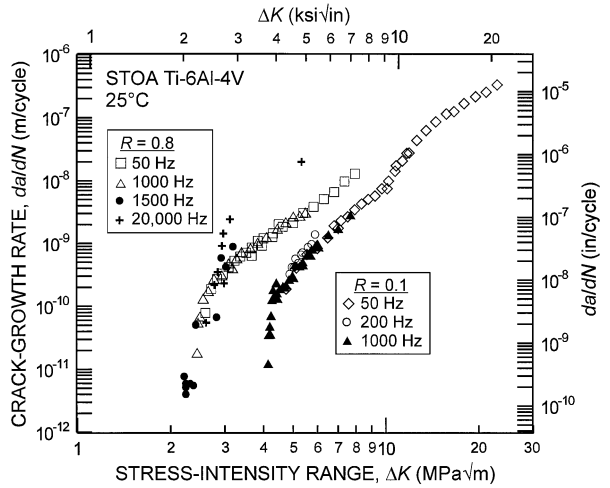

Fig. 5 Effect of test frequency on fatigue-crack propagation in Ti–6Al–4V in room air. Results from (large-crack) compact-tension tests at 50, 200 and 1000 Hz, notched tensile tests at 1500 Hz, and ultrasonic fatigue tests[20] at 20 000 Hz, show no statistically significant deviation in near-threshold behaviour.

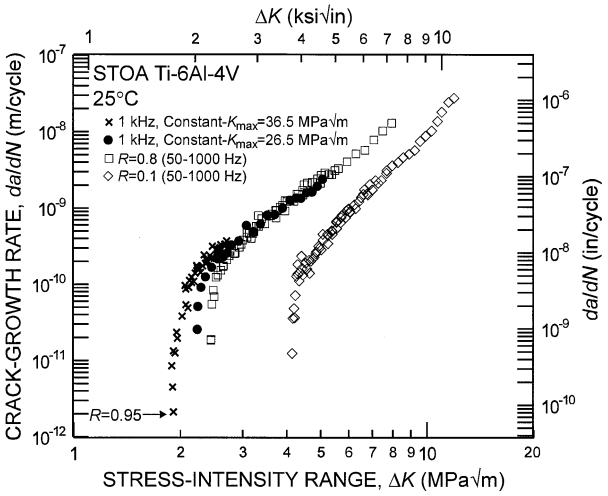

Fig. 6 Large-crack constant K_{max}/increasing K_{min} testing at 1000 Hz in room air on the solution-treated and overaged Ti–6Al–4V alloy was used to achieve $R = 0.95$, resulting in a lower-bound threshold of 1.9 MPa$\sqrt{m}$. Results are compared with constant R data at both 50 and 1000 Hz.

cracks in the same microstructure (see below), where small-crack growth was not observed below a ΔK of 2.9 MPa$\sqrt{\text{m}}$ ($R = 0.1$).[24]

Small-crack behaviour

Naturally initiated small-crack growth ($a \sim 45$–1000 μm) behaviour has been measured in this microstructure by Lütjering and co-workers using cylindrical tensile samples.[24] Results at $R = 0.1$ (with an applied maximum stress of 550 MPa and a frequency of 85 Hz) are compared in Fig. 7 with the present large-crack data at $R = 0.1$ and 0.8–0.95. Although the growth rates of the small cracks generally exceed those of the large cracks at the same applied ΔK level, no small-crack growth has been reported to date below $\Delta K \sim 2.9$ MPa$\sqrt{\text{m}}$. This value is 45% larger than the 'worst-case' ΔK_{TH} value of 1.9 MPa$\sqrt{\text{m}}$, measured with large cracks in this alloy at $R = 0.95$ using constant K_{max}/increasing K_{min} cycling.

Small-crack growth from simulated foreign object damage sites was also examined. A SEM micrograph of a typical impact site at 300 m/s is shown in Fig. 8 with a schematic illustration of the relevant features in the crater profile (for a more complete characterization of the damage, see Ref. [25]). The effect of the damage was to markedly reduce the fatigue life from that obtained with an undamaged sample, as shown in Table 1. Specifically, fatigue lives were reduced by over two orders of magnitude following 200 and 300 m/s impacts, with cracks tending to initiate at the bottom of the indent for

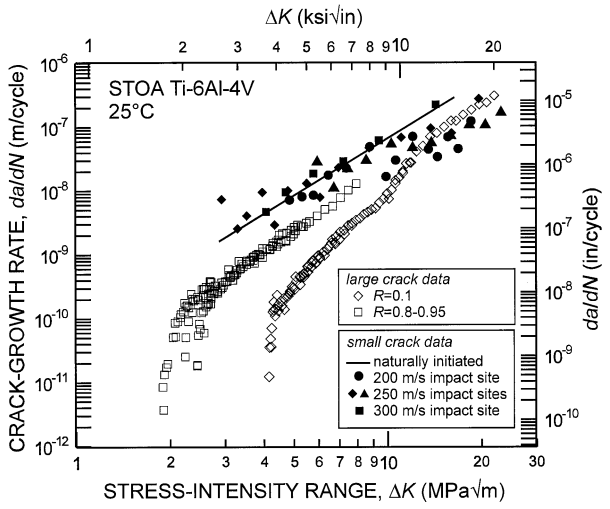

Fig. 7 Fatigue-crack propagation results for naturally initiated small ($\sim$45–1000 μm) surface cracks at $R = 0.1$ (line)[24] and for small cracks emanating from a variety of FOD impact sites (closed symbols) in the solution-treated and overaged Ti–6Al–4V alloy, as compared to through-thickness, large cracks (>5 mm) at $R = 0.1$ and 0.8–0.95. All measurements were made in room air.

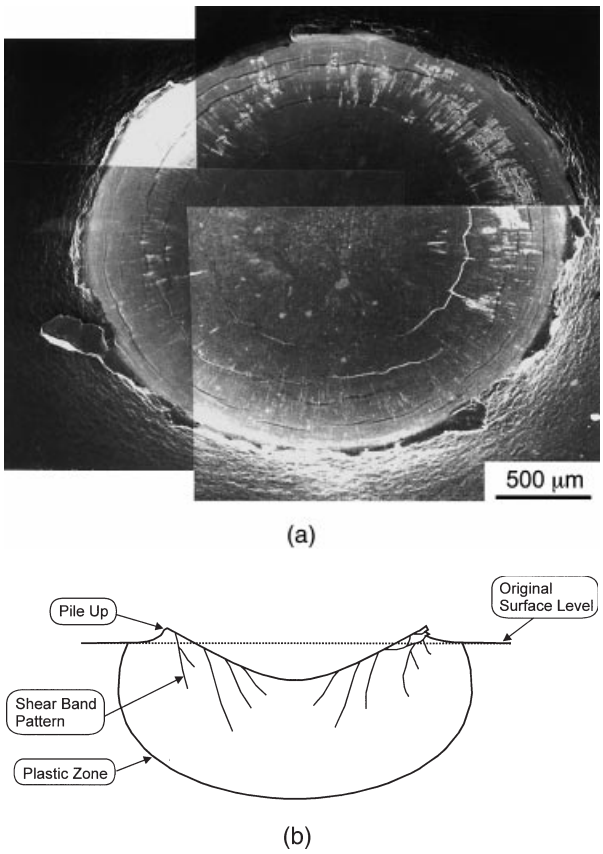

Fig. 8 Characteristics of surface damage due to impact: (a) SEM micrograph of simulated foreign object damage resulting from 90° impact by a hardened steel sphere with an incident velocity of 300 m/s; and (b) corresponding schematic illustrating features present at both 300 and 250 m/s. At 200 m/s, neither the shear bands nor the 'pile up' were observed.

Table 1 Summary of fatigue lives following simulated foreign object damage ($\sigma_{max} = 500$ MPa, $R = 0.1$, 20 Hz frequency)

	After 200 m/s FOD	After 300 m/s FOD	Smooth-bar undamaged sample
Initiation life	4.3×10^4	2.9×10^4	—
Total life	7.5×10^4	4.6×10^4	$>10^7$

the lower velocity impacts and at the crater rim for the higher velocity impacts.

The growth rates of the small cracks originating from such impact sites are also compared in Fig. 7 with growth rate data for large (>5 mm) and naturally initiated small ($\sim$45–1000 μm) cracks in this microstructure. Both the naturally initiated and FOD-initiated small-crack velocities were within the same scatter band, initially up to an order of magnitude faster than corresponding large-crack results (although small-crack data tended to merge with large-crack results above $\Delta K \approx 10$ MPa$\sqrt{\text{m}}$ as crack

sizes increased). However, in the limited data collected to date, no FOD-initiated cracks have been observed in the Ti–6Al–4V below a ΔK of $\sim 2.9\ \mathrm{MPa}\sqrt{\mathrm{m}}$; i.e. at a stress-intensity range above that of the 'worst-case', large-crack ΔK_{TH} threshold. It should be noted, however, that the residual stresses locally surrounding the FOD sites were not taken into account in plotting the FOD-initiated small-crack results. Such residual stresses are currently being analysed using synchrotron X-ray microdiffraction techniques.

Effect of environment

A comparison of fatigue-crack growth in Ti–6Al–4V at high frequencies (1–1.5 kHz) in ambient temperature air and vacuum ($\sim 10^{-6}$ torr) is shown in Fig. 9 at R ratios between 0.6 and 0.8. Although the threshold values are essentially unchanged ($\Delta K_{TH} \sim 2.6\ \mathrm{MPa}\sqrt{\mathrm{m}}$ in air versus $2.7\ \mathrm{MPa}\sqrt{\mathrm{m}}$ *in vacuo*), crack growth rates are some three orders of magnitude faster in air than *in vacuo*. In view of the observed absence of a frequency effect on growth rates between 50 and 20 000 Hz, the magnitude of the disparity in growth rates in air and vacuum is quite surprising. The origin of the apparent environmental contribution to crack growth is unclear at this time, but it may be associated with embrittlement due to hydrogen released by the reaction of the Ti with water vapour in the air,[26–28] or more probably with the role of oxygen in delocalizing plastic deformation, specifically by limiting the degree of slip reversibility at the crack tip.[29] The latter explanation is consistent with the rougher (macroscale) morphology of fatigue fracture surfaces in vacuum, as discussed below. However, as there is no effect of frequency on crack growth rates in air (between ~ 20 and 20 000 Hz), the environmental mechanism responsible for faster growth rates in air compared to vacuum must be extremely rapid. Along these lines, Gao *et al.*[28] have demonstrated that the rate of oxidation of Ti–5Al–2.5Sn in the presence of small amounts of water vapour (10^{-6} torr) is extremely rapid. Applying the derived oxidation reaction kinetics to the equilibrium partial pressure of water vapour at 25 °C ($p_{water} = 23.75$ torr), a clean surface of Ti–5Al–2.5Sn would be $\sim 90\%$ covered in oxide in 2.6×10^{-7} s. Thus, if slip-step oxidation was responsible for the observed dependence of fatigue-crack growth rates on the environment, one would not expect to see an effect of cyclic loading frequency on crack-propagation rates in air for all frequencies less than ~ 3.9 MHz, consistent with the current experimental results. However, given the fast nature of the oxidation process, it is likely that the surface reaction with H_2O is not the rate-limiting step. In fact, Gao *et al.*[28] suggest that the transport of the gas phase to the crack tip is rate limiting. Thus, a more realistic estimate of the critical frequency, above which slip-step oxidation will be suppressed in ambient air, requires a more detailed knowledge of the rate of water vapour transport to the crack tip.

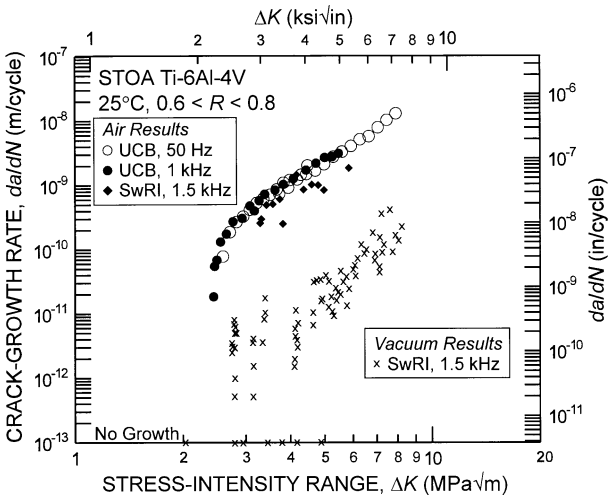

Fig. 9 Comparison of rates of fatigue-crack propagation in the solution-treated and overaged Ti–6Al–4V alloy at $R = 0.6$–0.8 and 1–1.5 kHz frequency in room air and vacuum ($\sim 10^{-6}$ torr). Note that although ΔK_{TH} threshold values are essentially unchanged, growth rates *in vacuo* are some three orders of magnitude slower than in air.

Mechanisms

There has been very little, if any, investigation of fatigue cracks growing below 10^{-9} m/cycle and at high load ratios. Therefore, fatigue-crack growth at rates in the range of 10^{-10}–10^{-12} m/cycle were observed *in situ* using a 1.5-kHz loading stage for a scanning electron microscope. Cracks were cycled in increments of between 200 000 cycles and 1 million cycles between measurements of crack length, depending on the loading variables.

At these low rates of propagation, fatigue cracks did not grow during every cycle, but rather would alternate between propagation and local arrest. With decreasing applied load, propagation became more intermittent until finally ceasing at the threshold. The criteria used for establishing this threshold was no growth at either end of a surface crack in 5 million cycles. When the fraction of increments in which growth was measured was correlated to ΔK, it was found that there was a transition period between a condition of no growth, presumably below ΔK_{TH}, and growth on each cyclic increment, which may be termed ΔK_{ss}. A fairly careful study of crack growth at two load ratios indicated that at $R = 0.85$, the transition period was over a small range

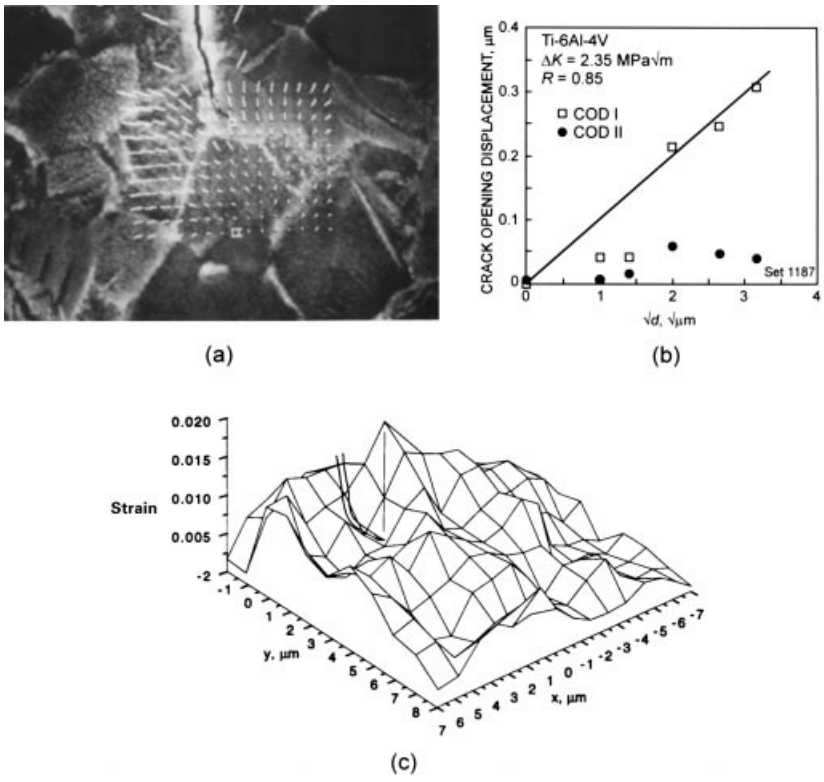

Fig. 10 (a) Crack-tip micromechanics are examined in a photograph of a crack growing at $R = 0.85$ at a rate of $\sim 10^{-11}$ m/cycle with displacements measured between minimum and maximum cyclic loads. (b) Crack-opening displacements (COD) in mode I and II measured from (a) (where the displacement interval is 1 μm and the displacements are magnified 15 times), as a function of the square root of the distance, *d*, behind the crack tip. (c) Maximum shear strain distribution in the region covered by the displacements. Strain is a maximum at the crack tip and the estimated size of the plastic zone is 2 μm.

of ΔK, while at $R = 0.5$, the range in ΔK over which growth was intermittent was larger.

The existence of a transition in ΔK between no growth and growth on each cyclic increment is similar to the change in slope of the da/dN–ΔK curve as ΔK is increased above ΔK_{TH}. At ΔK_{TH}, the slope of the curve is very steep. With increasing ΔK, the slope slightly decreases, and when ΔK_{ss} is reached, the curve assumes the slope of the Paris region, or the steady-state crack growth region.

Crack-tip micromechanics measurements were made for cracks growing at the low growth rates being studied. Only cracks growing *in vacuo* are discussed here because of the very large influence of an air environment on crack growth kinetics, and therefore on the mechanisms of crack growth.

Fatigue cracks were consistently found to be closed at the tip at the minimum cyclic load, although this closure in some of the observations extended only a few tens of micrometres. Crack-opening loads were found to be approximately half the cyclic load, even at $R = 0.85$. These observations are apparently inconsistent with the compliance-based closure measurements on large cracks in compact-tension samples, where no closure was detected above an *R*-ratio of ~ 0.5. However, compliance measurements are macroscopic and yield a global measure of crack-surface contact; it is unlikely that they would detect such local closure within 10 μm or so of the crack tip.

Photographs made at the minimum and maximum cyclic loads were analysed to determine the crack-opening displacement (COD) and crack-tip strain levels using the automated stereoimaging technique. An example of these measurements is shown in Fig. 10. This figure shows a photograph of the crack-tip region with the displacements overlayed. COD is shown in the upper right of the figure as a function of the square root of *d*, the distance behind the crack tip. From this relationship, the crack-tip opening displacement (CTOD) may be defined at 1 μm behind the tip.

The distribution of strain for crack tips at this high *R* does not seem to be much affected by the grain structure, although this point has not been extensively investigated. The plastic-zone size was determined by subtracting the elastic strain (twice the yield stress/modulus) from the total strain. The plastic-zone size for the crack tip shown in Fig. 10 extends ≈ 2 μm ahead of the crack tip. Plastic-zone sizes are of the order of the α particle size. Strains near the crack tip did not appear to be affected by the presence of α/α or α/β boundaries.

The correlation between CTOD (defined at 1 μm behind the crack tip) and crack-tip strain that has been found at lower *R* ratio[30] continues for high *R*, as shown in Fig. 11. The magnitude of the crack-tip strains under

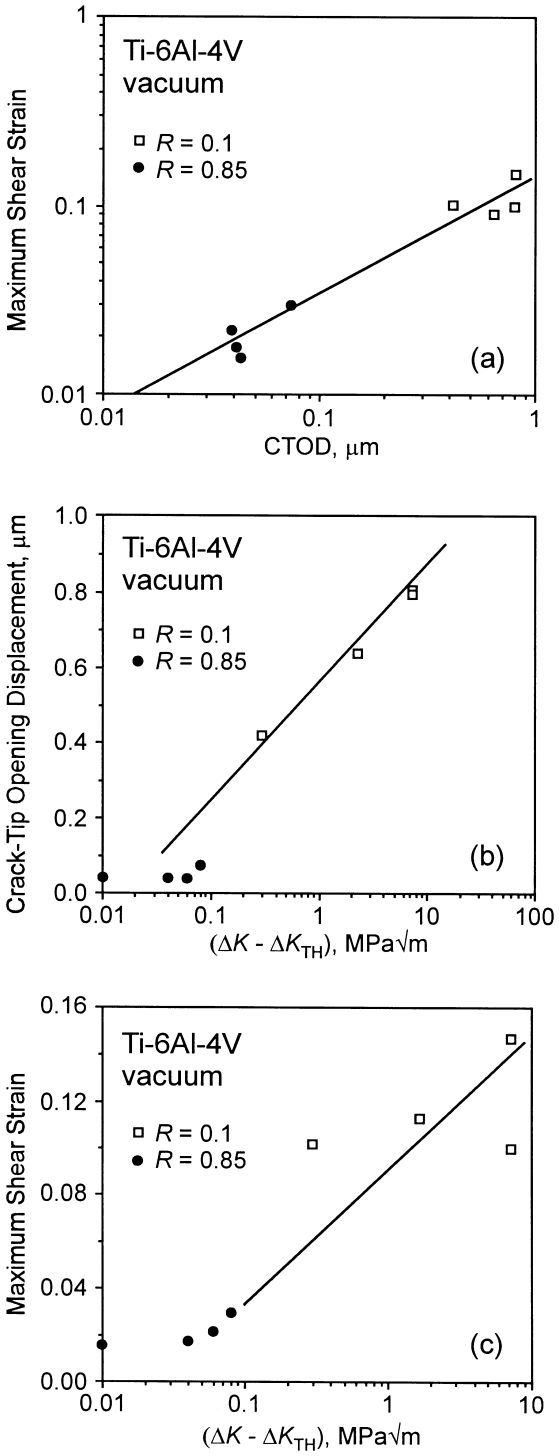

Fig. 11 Correlations between micromechanics and loading parameters are shown in the results obtained under HCF conditions ($R = 0.85$); these are compared with those previously obtained at low R.[30] (a) Maximum shear strain at the crack tip correlated with CTOD. (b) CTOD correlated with (ΔK–ΔK_{TH}). (c) Maximum crack-tip shear strain correlated with (ΔK–ΔK_{TH}).

these conditions was not always found to be above the elastic limit. This condition probably resulted from the fact that cracks were not growing during some increments of cycling. Also shown in Fig. 11 are the correlations between crack-tip strain and CTOD and the term (ΔK–ΔK_{TH}).

Fractography

Investigations of the fracture surfaces in the tensile fatigue samples indicated that the surface-crack profiles were approximately semicircular ($c/a \sim 1$), meaning that crack growth rates on the surface and interiors of the material were approximately the same. The surface topography produced at the very low crack growth rates investigated was examined using a field emission SEM. The high resolution and low beam voltage of the field emission SEM was necessary to reveal the very low level of topography existent on individual primary α grains and within individual lamellar colonies present at the fracture surfaces produced *in vacuo*; however, on a more macroscale, fracture surfaces in vacuum were distinctly rougher. Using this technique, some evidence of an incremental mechanism of fatigue-crack growth (striations) was found on the α grains. At a growth rate of 10^{-12} m/cycles, the average striation spacing on the surfaces of α particles was $\approx$50 nm, or there were 20 striations in 1 μm of growth. This means that under vacuum conditions, it required an average of 40 000 cycles to produce one striation. Clearly, *in vacuo*, the crack is not making one striation per loading cycle.

With a plastic-zone size of $\approx$2 μm ($\sim$100 times larger than the observed striation spacing), $\sim 2 \times 10^6$ cycles were needed for the crack to traverse the plastic zone when the average crack growth rate was 10^{-12} m/cycle. The volume of material in the plastic zone would therefore experience $\approx 2 \times 10^6$ cycles of loading, and it is likely that dislocation subcells would be formed during this large number of cycles near the crack plane, as has previously been found at higher ΔK in these alloys.

Worst-case threshold concept

The problem of turbine-engine high-cycle fatigue requires that design must be based on the notion of a threshold stress intensity for no crack growth under the appropriate conditions of high mean loads, ultrahigh frequency (vibratory) loading, and small-crack sizes. Because the measurement of small-crack thresholds is experimentally tedious and complex, one approach used in the current work has been to simulate the mechanistic origins of the small-crack effect using 'worst-case' large-cracks, i.e. the measurement of thresholds under conditions which simulate the similitude limitation of small

cracks by minimizing crack closure in the wake. Whereas this approach to simulate small-crack behaviour with large cracks might not be appropriate for truly microstructurally small cracks, where essentially any continuum measure of behaviour would be questionable, the crack sizes relevant to the Air Force HCF problem are expected to be somewhat larger, of the order of 50–100 μm and above. As described above, using constant K_{max}/increasing K_{min} cycling, the present results show the 'worst-case' threshold in Ti–6Al–4V, measured with large (>5 mm) cracks at very high load ratios ($R \sim 0.95$) and representative frequencies (1 kHz), to be $\Delta K_{TH} = 1.9\,\text{MPa}\sqrt{\text{m}}$. ΔK_{TH} thresholds tend to approach zero as $R \to 1$;[31] however, as the current value at $R = 0.95$ is defined as $K_{max} \to K_{Ic}$, in the apparent absence of global closure and below the stress intensities for the growth of naturally initiated small ($\sim$45–1000 μm) cracks and small cracks emanating from sites of foreign object damage, it is believed that the 'worst-case' threshold concept can be used as a practical lower-bound threshold for the stress intensity required for the onset of small-crack growth under HCF conditions.

CONCLUSIONS

Based on a preliminary investigation into the high-cycle fatigue of a solution-treated and overaged Ti–6Al–4V turbine-engine alloy tested in ambient temperature air and vacuum, the following conclusions can be made.

1 Ambient temperature fatigue-crack propagation (over the range $\sim 10^{-12}$–10^{-6} m/cycle) and threshold ΔK_{TH} values were found to be independent of test frequency over the range 50–1500 Hz, based on tests on servohydraulic and *in situ* SEM testing machines. Moreover, comparisons to the published results on a similar microstructure in Ti–6Al–4V strongly suggest that the frequency-independent behaviour extends out to 20 000 Hz, at least at near-threshold levels.
2 A 'worst-case' fatigue threshold, measured for large cracks at $R = 0.95$ under constant K_{max}/increasing K_{min} conditions was found to be $1.9\,\text{MPa}\sqrt{\text{m}}$ for this alloy. This should be compared with measurements on naturally initiated small cracks and FOD-initiated small cracks in the same microstructure, where small-crack growth was not reported below a ΔK value of $2.9\,\text{MPa}\sqrt{\text{m}}$.
3 Foreign object damage, simulated by hardened steel spheres impacted at 200–300 m/s on a flat surface, provides sites for the initiation of small fatigue cracks. At applied stresses some 10% below the smooth-bar, fatigue strength (at 10^7 cycles), crack-initiation lives were less than 4×10^4 cycles, many orders of magnitude shorter than in unimpacted samples. Subsequent small-crack growth from the damage sites was found to occur at rates considerably faster than large cracks subjected to the same applied ΔK level. No crack growth from FOD sites has been observed to date at ΔK values less than $2.9\,\text{MPa}\sqrt{\text{m}}$.
4 Fatigue-crack growth rates *in vacuo*, over the range $\sim 10^{-12}$–10^{-9} m/cycle, were found to be approximately three orders of magnitude slower than corresponding rates in room air; ΔK_{TH} threshold values, conversely, were essentially unchanged.
5 Fractographically, fatigue-crack growth at $\sim 10^{-11}$–10^{-12} m/cycle was found to be clearly intermittent, with evidence of near-tip crack-surface contact (i.e. within $\sim$10 μm or so of the crack tip) at load ratios as high as 0.85. Measured crack-tip strain distributions were essentially unaffected by the microstructure (e.g. by the grain structure and α/α and α/β boundaries).
6 The 'worst-case' fatigue threshold of $1.9\,\text{MPa}\sqrt{\text{m}}$, measured for large cracks at $R = 0.95$, was found to provide a practical lower bound to describe the onset of growth of small cracks ($a \sim$ 45–1000 μm), initiated naturally or from sites of foreign object damage, under HCF conditions in this alloy.

Acknowledgements

This work was supported by the US Air Force Office of Scientific Research under the auspices of the Multidisciplinary University Research Initiative on *High Cycle Fatigue* to the University of California at Berkeley under Grant no. F49620-96-1-0478; in addition, D.L.D. was supported by AFOSR Grant no. F49620-96-C-0037. B.L.B. would also like to acknowledge the support of the Hertz Foundation. Thanks are due to Prof. Dr G. Lütjering, Dr J. A. Hines and Dr J. O. Peters of the Technische Universität Hamburg-Harburg for their results on naturally initiated small cracks, and to Dr A. W. Thompson for several helpful discussions.

REFERENCES

1 Report of the AdHoc Committee on Air Force Aircraft Jet Engine Manufacturing and Production Processes (1992) United States Air Force Scientific Advisory Board, SAF/AQQS: the Pentagon, Washington, D.C.
2 B. A. Cowles (1996) High cycle fatigue in aircraft gas turbines—an industry perspective. *Int. J. Fracture* **80,** 147–163.
3 J. C. I. Chang (1996) An integrated research approach to attack engine HCF problems. Air Force Office of Scientific Research, Bolling AFB, Washington, D.C.
4 D. Taylor (1985) *A Compendium of Fatigue Thresholds and Crack Growth Rates*, EMAS, Warley, UK.

5 J. K. Gregory (1994) Fatigue crack propagation in titanium alloys. In: *Handbook of Fatigue Crack Propagation in Metallic Structures* (Edited by A. Carpinteri), Elsevier Science, Oxford, U.K., pp. 281–322.
6 J. M. Larsen, B. D. Worth, C. G. Annis and F. K. Haake (1996) An assessment of the role of near-threshold crack growth in high-cycle-fatigue life prediction of aerospace titanium alloys under turbine engine spectra. *Int. J. Fracture* **80,** 237–255.
7 R. O. Ritchie (1996) Small cracks and high-cycle fatigue. In: *Proceedings of the ASME Aerospace Division* (Edited by J. C. I. Chang, J. Coulter, D. Brei, D. Martinez, W. Hg and P. P. Freidmann), ASME, New York, NY, AMD, Vol. 52, pp. 321–333.
8 R. O. Ritchie and J. Lankford (1986) Small fatigue cracks: a statement of the problem and potential solutions. *Materials Sci. Engineering* **84,** 11–16.
9 D. Eylon (1998) Summary of the available information on the processing of the Ti–6Al–4V HCF/LCF program plates. University of Dayton Report, Dayton, OH, USA.
10 R. O. Ritchie and W. Yu (1986) Short crack effects in fatigue: a consequence of crack tip shielding. In: *Small Fatigue Cracks* (Edited by R. O. Ritchie and J. Lankford), TMS-AIME, Warrendale, PA, USA, pp. 167–189.
11 H. Döker, V. Bachmann and G. Marci (1982) A comparison of different methods of determining the threshold for fatigue crack propagation. In: *Fatigue Thresholds, Proceedings of the 1st International Conference* (Edited by J. Bäcklund, A. F. Blom and C. J. Beevers), EMAS, Warley, UK, Vol. 1, pp. 45–57.
12 W. A. Herman, R. W. Hertzberg and R. Jaccard (1988) Influence of mean stress on fatigue in several aluminium alloys utilizing K^{c}_{max} threshold procedures. *Fatigue Fract. Engng Mater. Struct.* **11,** 303–320.
13 J. M. Morgan and W. W. Milligan (1997) A 1 kHz servohydraulic fatigue testing system. In: *High Cycle Fatigue of Structural Materials* (Edited by W. O. Soboyejo and T. S. Srivatsan), TMS, Warrendale, PA, USA, pp. 305–312.
14 J. C. Newman, Jr and I. S. Raju (1981) An empirical stress-intensity factor equation for the surface crack. *Engng Fracture Mech.* **15,** 185–192.
15 M. D. Halliday and C. J. Beevers (1981) Some aspects of fatigue crack closure in two contrasting titanium alloys. *J. Testing Evaluation* **9,** 195–201.
16 K. S. Ravichandran (1991) Near threshold fatigue crack growth behavior of a titanium alloy: Ti–6Al–4V. *Acta Metall. Mater.* **39,** 401–410.
17 T. Ogawa, K. Tokaji and K. Ohya (1993) The effect of microstructure and fracture surface roughness on fatigue crack propagation in a Ti–6Al–4V alloy. *Fatigue Fract. Engng Mater. Struct.* **16,** 973–982.
18 S. Dubey, A. B. O. Soboyejo and W. O. Soboyejo (1997) An investigation of the effects of stress ratio and crack closure on the micromechanisms of fatigue crack growth in Ti–6Al–4V. *Acta Mater.* **45,** 2777–2787.
19 R. A. Schmidt and P. C. Paris (1973) Threshold for fatigue crack propagation and effects of load ratio and frequency. In: *Progress in Fatigue Crack Growth and Fracture Testing. ASTM STP 536*, pp. 79–94.
20 C. Bathias, K. El Alami and T. Y. Wu (1997) Influence of mean stress on Ti–6Al–4V fatigue crack growth at very high frequency. *Engng Fracture Mech.* **56,** 255–264.
21 R. J. H. Wanhill (1974) Environment and frequency effects during fatigue crack propagation in Ti–2.5Cu (IMI 230) sheet at room temperature. *Corrosion-NACE* **30,** 28–35.
22 D. B. Dawson and R. M. N. Pelloux (1974) Corrosion fatigue crack growth of titanium alloys in aqueous environments. *Metallurg. Trans.* **5,** 723–731.
23 C. F. Shih (1981) Relationships between the J-integral and the crack opening displacement for stationary and extending cracks. *J. Mech. Phys. Solids* **29,** 305–326.
24 J. A. Hines, J. O. Peters and G. Lütjering (1999) Microcrack propagation in Ti–6Al–4V. In: *Fatigue Behavior of Titanium Alloys* (Edited by R. Boyer, D. Eylon, J. P. Gallagher and G. Lütjering), TMS, Warrendale, PA, USA.
25 O. Roder, A. W. Thompson and R. O. Ritchie (1998) Simulation of foreign object damage of Ti–6Al–4V gas-turbine blades. In: *Proceedings of the Third National Turbine Engine High Cycle Fatigue Conference* (Edited by W. A. Stange and J. Henderson), Universal Technology, Dayton, OH, USA, CD-Rom, session 10, pp. 6–12.
26 D. A. Meyn (1971) An analysis of frequency and amplitude effects on corrosion-fatigue crack propagation in Ti–8Al–1Mo–1V. *Metallurg. Trans.* **2,** 853–865.
27 H. Döker and D. Munz (1977) Influence of environment on the fatigue crack propagation of two titanium alloys. In: *The Influence of Environment on Fatigue*, Mechanical Engineering Publications, London, UK, pp. 123–130.
28 S. J. Gao, G. W. Simmons and R. P. Wei (1984) Fatigue crack growth and surface reactions for titanium alloys exposed to water vapor. *Mater. Sci. Engng* **62,** 65–78.
29 M. Sugano, S. Kanno and T. Satake (1989) Fatigue behavior of titanium in vacuum. *Acta Metall.* **37,** 1811–1820.
30 D. L., Davidson and J. Lankford (1984) Fatigue crack growth mechanics for Ti–6Al–4V (RA) in vacuum and humid air. *Metallurg. Trans. A* **15A,** 1931–1940.
31 H. Döker (1997) Fatigue crack growth threshold: implications, determination and data evaluation. *Int. J. Fatigue* **19,** 5145–5149.